# Research Article

Synthesis, characterization, anti-microbial activity, and *in silico* assessment of a novel pyrazoline carboxamide heterocyclic compound

# Synthesis, characterization, antimicrobial activity, and *in silico* assessment of a novel pyrazoline carboxamide heterocyclic compound

## Farouk Boudou[1], Abdelghani Sehmi[2], Amal Belakredar[1] and Oussama Zaoui[3]

[1]Department of Biology, Faculty of Natural and Life Sciences, Djillali Liabes University of Sidi-Bel-Abbes, Sidi-Bel-Abbes 22000, Algeria; [2]Department of Natural and Life Sciences, Faculty of Sciences and Technology, University of Tissemsilt, Tissemsilt 38000, Algeria; [3]Department of Chemistry Faculty of Science, Kasdi Merbah University, BP 511, Ouargla 30000, Algeria.

## Abstract

This study presents the synthesis, characterization, and antimicrobial efficacy of a novel pyrazoline carboxamide heterocyclic compound. Synthesized through a two-step process, involving the formation of an α,β-unsaturated ketone and subsequent conversion into a pyrazoline carboxamide derivative, the compound's structure and functional groups were confirmed using FT-IR, $^1$H NMR, and DEPT-135 techniques. The compound demonstrated high purity and yield, displaying significant inhibitory zones against microorganisms, notably *Listeria monocytogenes* (14.2 ± 0.0 mm to 16.8 ± 1.3 mm) and *Candida albicans* (10.9 ± 0.6 mm to 17.8 ± 1.5 mm). Evaluation of drug-likeness and toxicity highlighted its potential for drug development. Molecular docking studies indicated strong binding affinities to key antimicrobial target proteins, including DNA gyrase, penicillin-binding protein, and *C. albicans* sterol 14-α-demethylase. Molecular dynamics simulations revealed the compound's structural flexibility. These results make this new compound a candidate for further exploration in drug development, highlighting its potential therapeutic applications.

## Introduction

Microorganisms have a profound impact on the world, affecting food cycles and human health. Within their realm, both non-pathogenic and pathogenic strains exist, each with distinct effects on living organisms (Wan-Mohtar et al., 2022). Non-pathogenic microorganisms are essential for ecological processes, nutrient cycling, and symbiotic relationships that aid digestion and vitamin synthesis, highlighting their vital role in sustaining life (Daisley et al., 2021). On the other hand, pathogenic microorganisms can cause infectious diseases by exploiting human immune system vulnerabilities. To combat them, antimicrobial agents like antibacterials, antivirals, and antifungals have been developed. Unfortunately, the improper use and excessive utilization of antimicrobial agents have led to a pressing issue: the emergence of antimicrobial resistance (Li and Webster, 2018). The rise of emerging and reemerging diseases presents a formidable challenge, compelling scientists to urgently search for new antimicrobial treatment to address resistant microorganisms (Aslam et al., 2018).

The search for highly potent molecules with exceptional therapeutic potential is increasing (Chen and Bajorath, 2023). Among these, pyrazole derivatives have emerged as a fascinating chemical entity with diverse biological activities and great promise for drug development (Brown, 2018). Their unique molecular structures and wide range of biological properties have attracted attention in the field of medicinal chemistry, making them a

subject of great interest and exploration (Ebenezer et al., 2022). The addition of the 5-(4-(dimethylamino)phenyl)-3-phenyl-4,5-dihydro-1H-pyrazole-1-carboxamide moiety has significantly enhanced the structural diversity and biological potential of pyrazolines, opening up interesting therapeutic prospect (Ebenezer et al., 2022).

The present researches highlighted the synthesis, spectroscopic characterization and antimicrobial activity of novel pyrazoline derivative 5-(4-(dimethylamino)phenyl)-3-phenyl-4,5-dihydro-1H-pyrazole-1-carboxamide (Pyr). In the last phase of this study, an in-depth *in silico* analysis was conducted to elucidate the potential antimicrobial mechanisms of the novel heterocyclic compound pyrazoline carboxamide.

## Materials and Methods

### Chemicals and reagents

The starting materials, reagents, solvents, and microbiological culture media were purchased from Sigma-Aldrich (USA) and Merck (Germany) and used without additional purification.

### Thin-layer chromatography

Analytical thin-layer chromatography (TLC) was conducted using pre-coated silica gel plates (60 F254, Merck) with cyclohexane:ethyl acetate (9.5:0.5, v/v) as the mobile phase. Following development, the plate was air-dried, and the separated components were visualized using iodine ($I_2$) for enhanced detection (Venkataraman et al., 2010).

### Synthesis of 5-(4-(dimethylamino)phenyl)-3-phenyl-4,5-dihydro-1H-pyrazole-1-carboxamide

In the initial step, the intermediate α,β-unsaturated ketone (chalcone derivative) was synthesized according to the reported procedure (Sehmi et al., 2020). An aqueous solution of sodium hydroxide (1.3 g, 0.032 mol) was added dropwise to a stirred solution of 4-(dimethylamino)benzaldehyde (2.5 g, 0.016 mol) and acetophenone (2.0 g, 0.016 mol) in ethanol. The reaction mixture was stirred at room temperature overnight. The precipitate was filtered, and washed with cold water until neutral pH was obtained, the crude solid was dried and then recrystallized in ethanol. The subsequent step involved the synthesis of pyrazoline carboxamide derivative. To a stirred ethanolic solution of chalcone derivative (2 g, 0.008 mol) and semicarbazide hydrochloride, (0.97 g, 0.008 mol), sodium hydroxide (0.7 g, 0.017 mol) in ethanol was added dropwise. The reaction mixture was refluxed for 6-7 hours. The reaction progress was monitored for chalcone disappearance by TLC using ethyl acetate/hexane mixture (1:3). After completion, the reaction mixture was cooled down and then poured on crushed ice to get the yellow precipitate that was later recrystallized with ethanol and chloroform mixture (8:2).

### Characterization methods

Melting points of the synthesized compound were determined by a Köfler hot-stage apparatus (Wagner & Munz, Germany).

The FT-IR measurements were carried out at room temperature using JASCO 4000 made in Japan. The spectrum was collected by the KBr-discs method in the infrared spectral range of 4000-400 cm-1 with a resolution of 4 cm-1.

---

**Box 1: Antibacterial and antifungal activity**

**Principle**

The agar diffusion method was employed to assess both antibacterial and antifungal activities.

**Requirements**

Incubator, Mueller-Hinton agar (2% beef extract, 17.5% acid hydrolysate of casein, 1.5% starch, and 1.5% agar), Sabouraud agar medium (1% yeast extract, 2% peptone, 2% dextrose, and 2% agar) Plate, Sterile swab, Test pathogens *Escherichia coli* ATCC 25922, *Staphylococcus aureus* ATCC 25923, *Pseudomonas aeruginosa* ATCC 27853, and *Listeria monocytogenes* ATCC 15313, *Candida albicans* ATCC MYA-2876

**Procedure**

*Step 1:* Gram-positive and Gram-negative bacteria obtained from 24-hour cultures and suspended in sterile saline to achieve concentrations of approximately $10^8$ CFU/mL relative to 0.5 McFarland standard. A suspension of Candida albicans (1 × $10^6$ cells/mL) in saline water was prepared for fungal culture

*Step 2:* Plates were prepared using 20 mL sterile Mueller-Hinton agar (2% beef extract, 17.5% acid hydrolysate of casein, 1.5% starch, and 1.5% agar) for antibacterial activity and Sabouraud agar medium (1% yeast extract, 2% peptone, 2% dextrose, and 2% agar) for antifungal activity

*Step 3:* The surface of the plates was inoculated with a sterile swab containing the saline suspension of bacteria and allowed to dry.

*Step 4:* Previously prepared wells, 6.0 mm in diameter, containing 50 uL of a methanolic solution of test compound of different concentrations, were placed on the agar surface.

*Step 5:* The antibiotic discs (gentamicin, pipemidic acid, cefazolin, and colistin) of 6.0 mm diameter, containing 10 to 50 µg of active substance per disc were placed on the agar surface

*Step 6:* The plates were then incubated at 37ºC and after 24 hours, clear zones of inhibition were observed around the disks and measured using a caliper.

**References**

Ignatov, 2021; Lake et al., 2023; Vică et al., 2021;

**References (Video)**

Rattanasuk et al., 2021; Sundar and Arunachalam, 2023

NMR experiments (^{1}H NMR and DEPT-135) were recorded at room temperature on a Bruker AC300 instrument using DMSO-d[6] as a solvent and TMS as an internal standard. Chemical shifts (δ) and coupling constants (J) are reported in ppm, and Hz, respectively.

### In silico drug-likeness and toxicity predictions

The SwissADME platform (http://www.swissadme.ch/index.php) was used to provide insights into ADME (Absorption, Distribution, Metabolism, and Excretion) parameters, pharmacokinetic properties, drug-likeness attributes, and the suitability of compounds from a medicinal chemistry perspective (Daina et al., 2017). The assessment of toxicity was carried out using the eMOLTOX web tool, which identified potential toxicities by analyzing various components within the drug (Ji et al., 2018).

### Molecular docking analysis

The ligand pyrazoline carboxamide was designed using Marvin Sketch Version 5.10.0 and saved in .pdb format. Ampicillin (CID: 6249) and clorobiocin (CID: 54706138) used as control ligands (antibiotics) were obtained from the PubChem database (www.pubchem.ncbi.nlm.nih.gov). These files were then processed with AutoDock tools to generate pdbqt files for molecular docking using AutoDock vina (Trott and Olson, 2010). The crystal structures of the target proteins, DNA gyrase (PDB ID: 1KZN) and PBP4 (PDB ID: 3HUN, PDB ID: 7KCY), and CYP51 (PDBID: 5TZ1) were obtained from the website www.rcsb.org. Water molecules were removed, and hydrogen atoms were added to the protein structure. Docking calculations were performed using AutoDock vina integrated into PyRx virtual screening tool v.8. The suitable binding area was adjusted around the active binding pockets of the proteins using the AutoGrid tool integrated into PyRx where the ligands can search for better binding with minimum energy by allocating x, y, and z-axis with suitable spacing. For the DNA gyrase, the grid box was set to 25 Å × 25 Å × 25 Å centered at 19.5403, 19. 16072, 43.3421 (X, Y, Z coordinates), for PBP4 the grid box, was set to 25 Å × 25 Å × 25 Å centered at -33.6029, 5.6410, -18.1544 (X, Y, Z coordinates), and for CYP51 the grid box was set to 25 Å × 25 Å × 25 Å centered at 6.5230, 7.9811, 11.0620 (X, Y, Z coordinates). The docking analysis was conducted on Microsoft Windows 10 professional version, service pack 3 with an Intel (R) i3-7020U CPU @ 2.30 GHz and 4.0 GB of RAM. BIOVIA Discovery studio visualizer 2021 was used to analyze the obtained conformations of the complex for binding energy and docking arrangements.

### Molecular dynamics simulation

To analyze the stability and movement of the protein-ligand combinations, the docking arrangements were subjected to molecular dynamics simulations. These simulations were performed using the iMODS server, accessible at http://imods.chaconlab.org (López-Blanco et al., 2014). The iMODS server assumes a critical role in investigating diverse patterns of movement and generating potential pathways of transition between proteins that are structurally akin. Among its functionalities, the iMODS server assesses protein stability by computing the internal coordinates of the protein through normal mode analysis (NMA). This server employs various measures to depict protein stability, encompassing a plot of mainchain deformability, B-factor readings, eigenvalues, covariance matrix, and an elastic network model.

### Statistical analysis

The results were obtained in triplicate (n=3) and presented as the mean ± standard deviation. Statistical analysis was performed using Sigma-Plot for Windows version 11.0. Statistical significance was performed by a one-way ANOVA (analysis of variance) test followed by a post-hoc Tukey test.

## Results

### Synthesis of 5-(4-(dimethylamino)phenyl)-3-phenyl-4,5-dihydro-1H-pyrazole-1-carboxamide

The titled compound was obtained in good yield (1.9 g, 77%). The melting point was 184-186°C.

### Characterization

The resulting ^{1}H NMR spectrum exhibited a singlet signal at the chemical shift δ 2.8 ppm corresponding to H22 and H23 protons of the dimethylamino group (Figure 1). The spectrum confirmed the pyrazoline ring formation due to the appearance of three doublet of doublet at the chemical shifts δ 3.0-3.07 ppm (dd, J = 17.7, 4.9 Hz, 1H), δ 3.7-3.8 ppm (dd, J = 17.7, 11.9 Hz, 1H) and δ 5.2-5.3 ppm (dd, J = 11.9, 4.9 Hz, 1H), respectively referred for H1 and H3. The singlet signal resonated at δ 6.31 ppm assigned to H20 of the carboxamide entity and the multiplet signals observed in different integrals ratios between δ 6.6 and δ 7.8 ppm were attributed to aromatic protons.

The DEPT-135 spectrum showed a signal at the chemical shifts δ 40.2-41.1 ppm referred to C22 and C23 carbons of the dimethylamino group (Figure 2). The spectrum confirmed the successful cyclization of the pyrazoline ring by the appearance of a negative peak at δ 67.4-64.1 ppm and a positive peak at δ 59.7 ppm, respectively assigned to C1 and C2 carbons.

Fourier transform infrared spectroscopy (FTIR) of the title compound showed an intense peak at 1674 cm^{-1} assigned to the C=O band and a wide band at 3470 cm^{-1} referring to the N-H band of the carboxamide entity (Figure 3). The C-H band of phenyl ring hybridized sp[3] was observed at 2910 cm^{-1} and that pyrazoline ring hybridized sp[2] appeared at 2805 cm^{-1}.
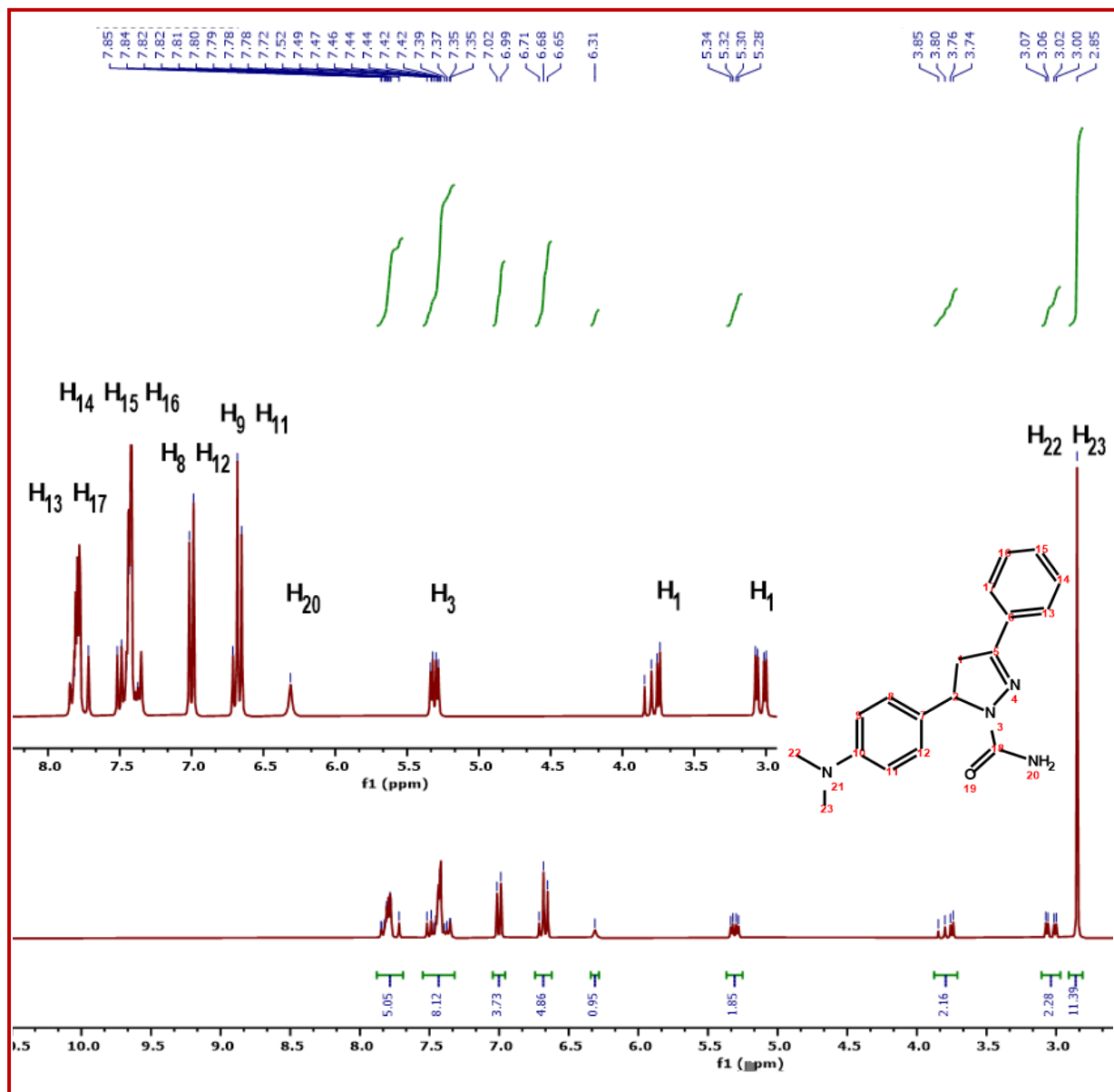
Figure 1: ¹H NMR spectrum of the pyrazoline carboxamide compound

### Antimicrobial activity

The results showed varying degrees of inhibition against the tested microorganisms at different concentrations of pyrazoline carboxamide (Table I). *E. coli* showed moderate sensitivity towards the synthesized compound, with zones of inhibition ranging from 11.3 ± 0.1 mm to 13.8 ± 0.8 mm for the concentrations tested. *S. aureus* showed a similar response, with zones of inhibition ranging from 10.9 ± 0.7 mm to 14.1 ± 0.2 mm. Notably, *L. monocytogenes* showed greater sensitivity to pyrazoline carboxamide, with zones of inhibition ranging from 14.2 ± 0.0 mm to 16.8 ± 1.3 mm. whereas, *P. aeruginosa* showed a moderate response, with zones of inhibition ranging from 11.2 ± 0.0 mm to 12.8 ± 1.1 mm. In contrast, *C. albicans* showed notable sensitivity to

pyrazoline carboxamide, with zones of inhibition ranging from 10.9 ± 0.6 mm to 17.8 ± 1.5 mm. Comparatively, the selected antibiotics showed variable levels of inhibition. Gentamicin showed significant inhibition against *E. coli* (31.8 ± 0.2 mm) and *S. aureus* (18.9 ± 0.4 mm). Piephemidic acid showed moderate inhibition against *S. aureus* (14.6 ± 0.3 mm), while cefazolin showed moderate inhibition against *S. aureus* (28.9 ± 0.8 mm) and *P. aeruginosa* (26.2 ± 1.6 mm). Colistin showed limited efficacy, with a zone of inhibition of 13.2 ± 0.1 mm against *P. aeruginosa*.

### Drug-likeness and toxicity predictions

The synthesized novel pyrazoline carboxamide compound exhibited a promising profile based on the comprehensive data analysis provided by the Swiss-
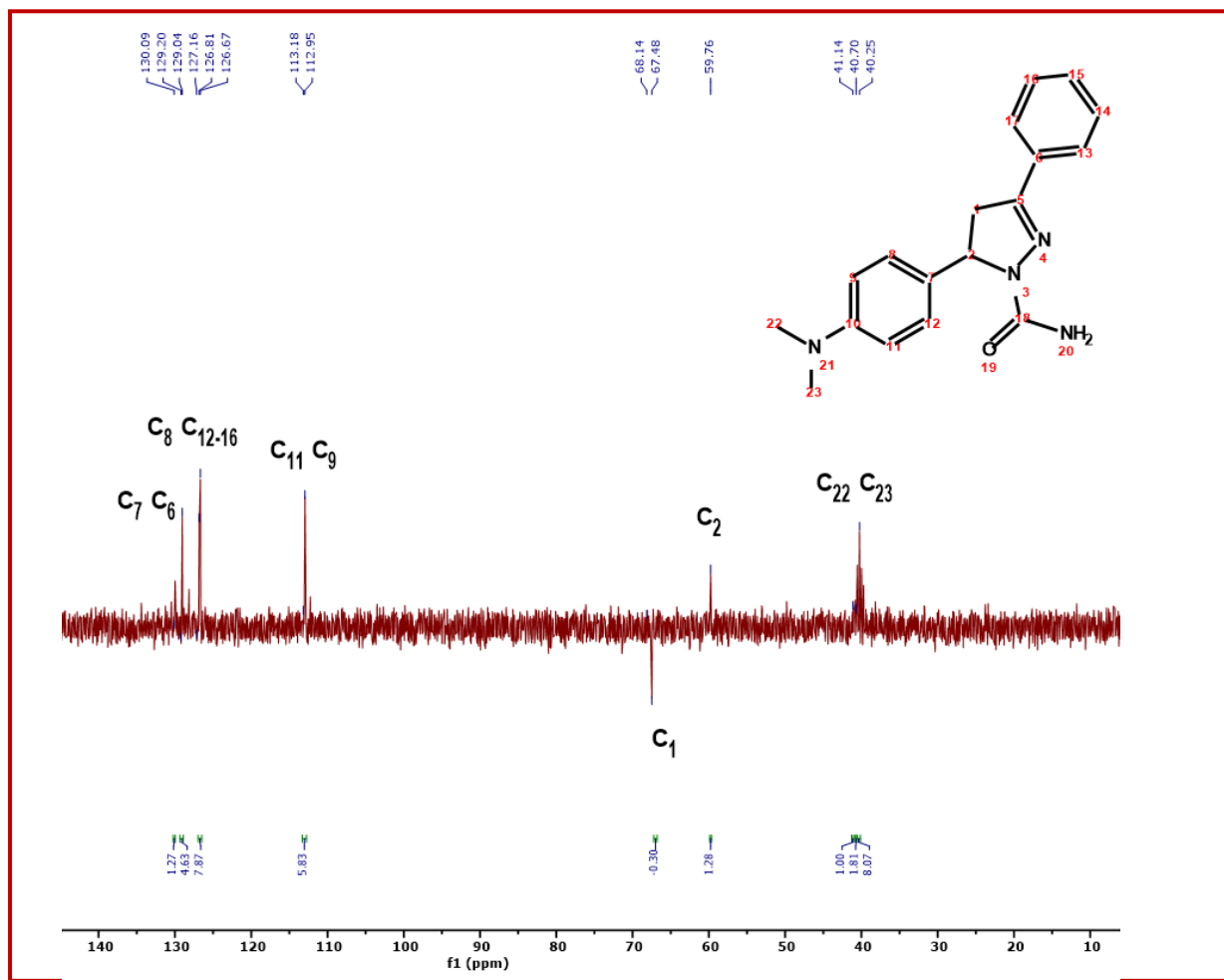
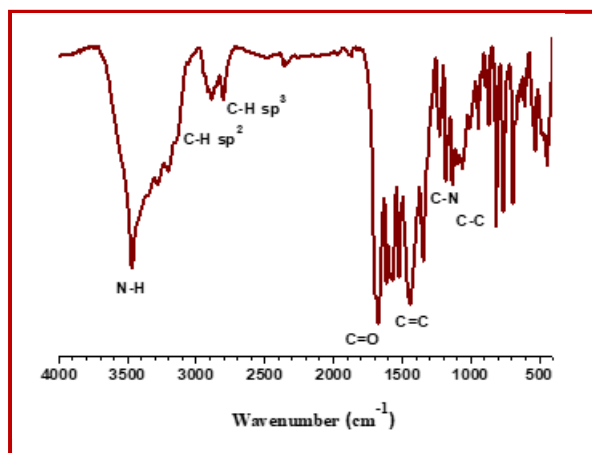Figure 2: DEPT-135 spectrum of the pyrazoline carboxamide compound



Figure 3: FT-IR spectrum of the pyrazoline carboxamide compound

ADME platform (Supplementary Table I). Its physico-chemical attributes, including molecular weight, composition, and aromaticity, position it within a molecular framework that could be favorable for drug development. The relatively low fraction of sp3 hybrid-dization (Csp3) might suggest a balance between aromatic and aliphatic components, potentially influencing its interactions and reactivity. The compound's lipophilicity, as indicated by various Log Po/w values, suggests a moderate affinity for both aqueous and lipid environments. This could have implications for its distribution within the body and its potential to permeate biological membranes. Furthermore, the compound's solubility characteristics, spanning a range of methods, underline its ability to dissolve in aqueous solutions, which is essential for effective delivery and absorption. In terms of pharmacokinetics, the compound's high gastrointestinal absorption and blood-brain barrier permeation potential hint at its ability to effectively enter the systemic circulation and potentially target the central nervous system. The non-substrate status for P-glycoprotein is encouraging, as it suggests reduced susceptibility to efflux transporters that can impede drug absorption (Figure 4). However, its interactions with various cytochrome $P_{450}$ enzymes, including inhibition of CYP2C19 and CYP2C9, warrant careful consideration in terms of drug interactions and metabolic pathways. The compound's favorable drug-

| Table I | | | | | | |
|---|---|---|---|---|---|---|
| **Inhibition zones of pyrazoline carboxamide and selected antibiotics against tested microorganism strains** | | | | | | |
| | | Inhibition zone (mm) | | | | |
| Synthetized compound/antibiotics | Concentration | *Escherichia coli* | *Staphylococcus aureus* | *Listeria monocytogenes* | *Pseudomonas aeruginosa* | *Candida albicans* |
| Pyrazoline carboxamide | 5000 µg/mL | 13.8 ± 0.8[a] | 13.2 ± 0.0[a] | 16.8 ± 1.3[b] | 11.4 ± 0.4[c] | 17.8 ± 1.5[b] |
| | 2500 µg/mL | 11.8 ± 0.2[a] | 12.2 ± 0.0[a] | 15.3 ± 0.0[b] | 12.8 ± 1.1[b] | 13.8 ± 0.7[b] |
| | 1250 µg/mL | 11.3 ± 0.1[a] | 14.1 ± 0.2[b] | 15.4 ± 0.4[c] | 12.0 ± 0.2[a] | 10.9 ± 0.6[a] |
| | 630 µg/mL | 12.1 ± 0.4[a] | 10.9 ± 0.7[a] | 14.2 ± 0.0[b] | 11.2 ± 0.0[a] | 11.3 ± 0.3[a] |
| | 312 µg/mL | 13.4 ± 0.6[a] | 12.8 ± 0.7[a] | 16.3 ± 0.9[b] | 11.7 ± 0.4[b] | 11.5 ± 0.5[c] |
| Gentamicin | 50 µg/disc | 31.8 ± 0.2[a] | 18.9 ± 0.4[b] | 32.1 ± 4.9[c] | 35.7 ± 0.0[c] | nil |
| Pipemidic acid | 30 µg/disc | 13.9 ± 0.4[a] | 14.6 ± 0.3[a] | nil | nil | nil |
| Cefazolin | 20 µg/disc | nil | 28.9 ± 0.8[a] | nil | 26.2 ± 1.6[a] | nil |
| Colistin | 10 µg/disc | nil | nil | nil | 13.3 ± 0.2 | nil |
| Data are mean ± SD; n=3; The superscripts (a-e) indicate: Values that share the same superscript letters do not differ significantly, while those do not share the same letter differ significantly | | | | | | |

likeness properties, passing multiple filters including Lipinski's rule of five and others, indicate its potential suitability as a drug candidate. Moreover, its bioavailability score falls within a moderate range, suggesting that its pharmacokinetic properties align reasonably well with expectations for efficient drug delivery and exposure. In the realm of medicinal chemistry, the presence of PAINS alerts raises concerns about potential interference in biological assays and requires thorough investigation. However, the compound's adherence to lead likeness criteria and its moderate synthetic accessibility score suggest feasible pathways for further

development. Toxicity assessment utilized the eMOLTOX web tool, analyzing various drug components (Figure 5). The tool provided a concise safety indication for human use, despite strong therapeutic properties. Data-driven models revealed no detected toxic actions. However, the eMOLTOX tool identified potential toxic substructures in the molecular representation. These included idiosyncratic toxicity with metabolic activation, an unpredictable adverse reaction linked to the body's metabolism converting the drug into harmful compounds, covalent bonds with DNA forming strong, permanent connections that could
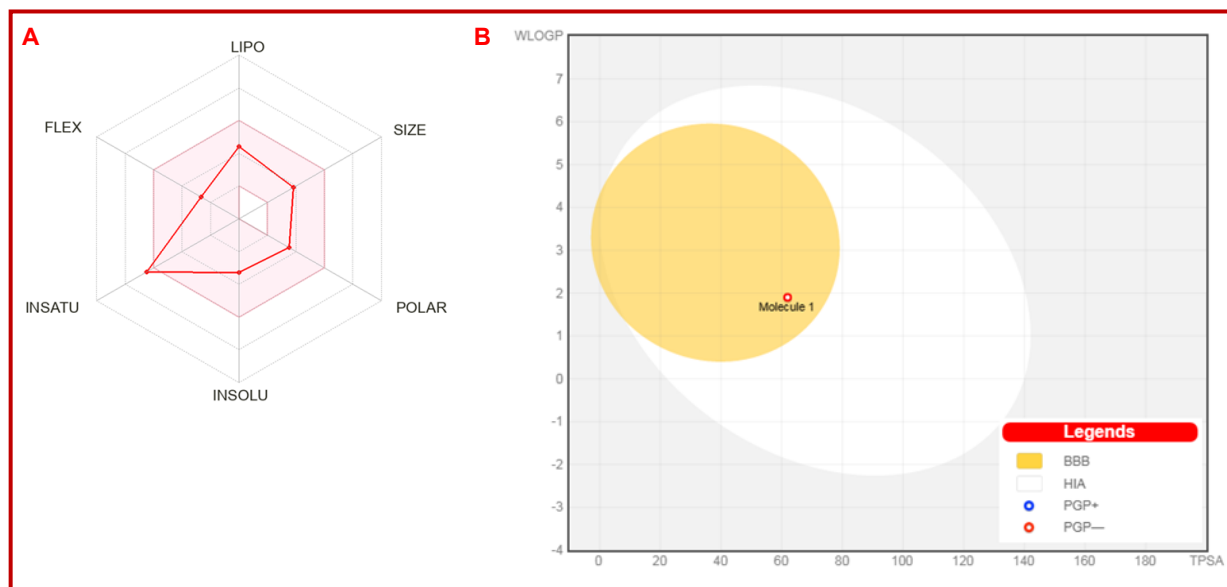


Figure 4: Oral bioavailability graph from the SwissADME database. The colored zone indicates the physicochemical space for oral bioavailability, and the red line defines the oral bioavailability properties of Pyr (A). Boiled-egg plot from the SwissADME database reveals human-blood–brain barrier absorption and the red dot indicates that the molecule is predicted not to be effluent from the central nervous system by p-glycoprotein (B). LIPO: lipophilicity, POLAR: polarity, INSOLU: insolubility, INSATU: unsaturation, FLEX: flexibility, BBB: blood–brain barrier, HIA: human intestinal absorption, PGP+: p-glycoprotein substrate, and PGP-: not a p-glycoprotein substrate

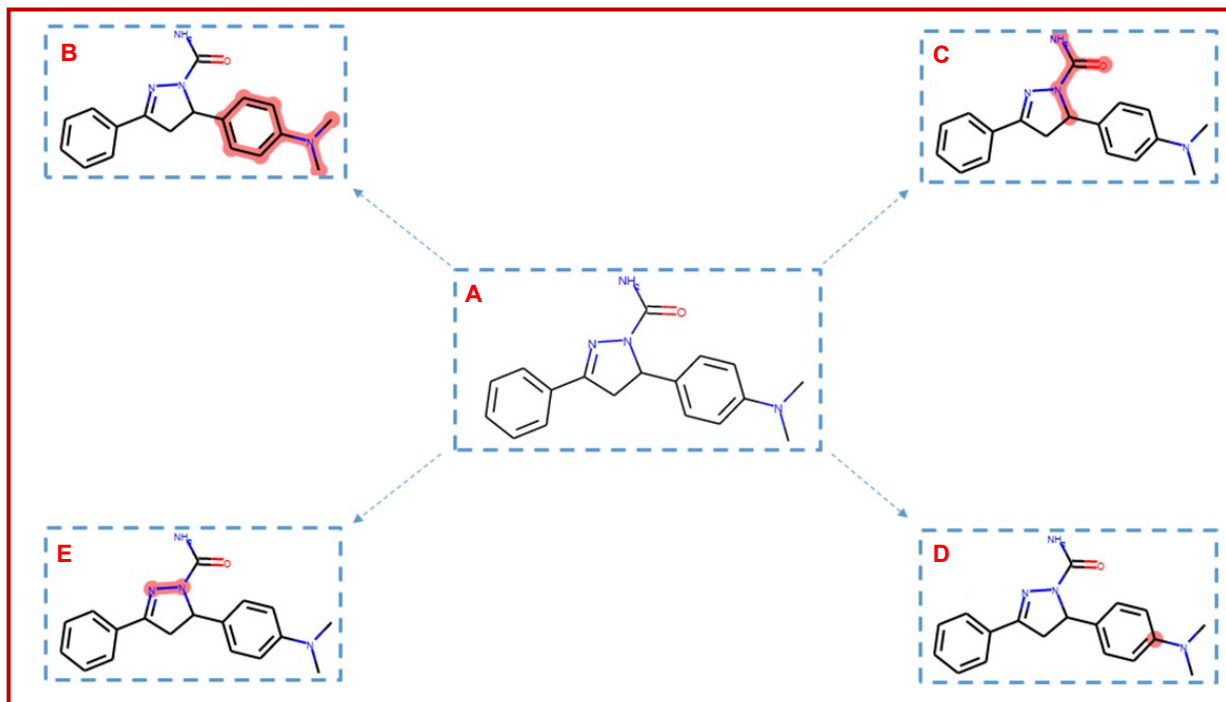Figure 5: Potential toxicity prediction of the novel pyrazoline carboxamide and its eventual toxic substructures (highlighted in red). Molecule depiction (A). Idiosyncratic toxicity (B). Covalent binds with DNA (C and D). Hepatotoxicity (E)

interfere with replication or transcription, and toxic substructures associated with hepatotoxicity (Figure 5).

*Molecular interaction assessment*

Examining the data, in the context of the protein with PDB ID 1KZN, pyrazoline carboxamide demonstrated a binding affinity of -7.9 kcal/mol (Table II). The interaction involved specific residues, including Asp A:49, Glu A:50, Gly A:77, and Ile A:78. In contrast, the reference standard inhibitor, clorobiocin, boasts a slightly enhanced binding affinity of -8.2 kcal/mol. The engagement

of clorobiocin entailed a distinct set of residues, such as Ile A:48, Leu A:52, Gly A:117, Asn A:46, Val A:43, Val A:120, Val A:167, Gly A:77, Glu A:42, and Asp A:49. Turning to the protein with PDB ID 3HUN, Pyr's interaction was characterized by binding energy of -7.9 kcal/mol, involving residues like Lys A:221, Ala B:129, and Asp B:130. Comparatively, the standard inhibitor ampicillin showed a binding affinity of -7.4 kcal/mol, with residues Thr B:232, Lys B:221, Leu A:96, and Lys A:221 implicated in the interaction. For the protein identified by PDB ID 7KCY, Pyr's affinity of -5.6 kcal/

| Table II | | | |
|---|---|---|---|
| Binding affinity and molecular interactions of four antimicrobial target proteins with a novel pyrazoline carboxamide and their respective standard inhibitors | | | |
| PDB ID | Ligands | Estimated free energy of binding (kcal/mol) | Residues involved in bonded interaction |
| 1KZN | Pyr (Designed) | -7.9 | Asp A:49, Glu A: 50, Gly A:77, Ile A: 78 |
| | Clorobiocin (CID: 54706138) | -8.2 | Ile A:48, Leu A:52, Gly A:117, Asn A:46, Val A:43, Val A:120, Val A:167, Gly A:77, Glu A:42, Asp A:49 |
| 3HUN | Pyr (Designed) | -7.9 | Lys A:221, Ala B: 129, Asp B: 130 |
| | Ampicillin (CID: 6249) | -7.4 | Thr B:232, Lys B: 221, Leu A:96, Lys A:221 |
| 7KCY | Pyr (Designed) | -5.6 | Gln A:57, Arg A:280, Lys A: 275, Leu A 223, Pro A:220 |
| | Cefoxitin (CID: 441199 ) | -4.3 | Ile A:216, Asp A:256, Lys A275 |
| 5TZ1 | Pyr (Designed) | -8.4 | Glu A:420, Tyr A: 69, Tyr A: 408, Thr A411, Gln A: 77 |
| | Oteseconazole (CID: 92132724) | -8.3 | Lys B:499, Glu B: 420, Val B:500, His B:373, Met B:374, Met B:372, Val B:510, Pro B:503, Asp B:502 |

mol was observed through interactions with residues Gln A:57, Arg A:280, Lys A:275, Leu A:223, and Pro A:220. In contrast, the standard inhibitor cefoxitin exhibited a binding energy of -4.3 kcal/mol, involving residues Ile A:216, Asp A:256, and Lys A:275. Lastly, with regards to the protein denoted by PDB ID 5TZ1, pyrazoline carboxamide demonstrates a notably strong affinity of -8.4 kcal/mol. The interaction centers around residues Glu A:420, Tyr A:69, Tyr A:408, Thr A:411, and Gln A:77. Comparatively, the standard inhibitor otese-conazole showed a binding energy of -8.3 kcal/mol, engaging residues Lys B:499, Glu B:420, Val B:500, His B:373, Met B:374, Met B:372, Val B:510, Pro B:503, and Asp B:502.

*Molecular dynamics study*

The NMA analysis of docked complexes (1KZN-Pyr, 3HUN-Pyr, 7KCY-Pyr, and 5TZ1-Pyr) revealed distinct mobility profiles, with complex 1KZN-Pyr displaying the highest deformability (Supplementary Figure 1). B-factor diagrams compare NMA and PDB fields, show-ing fluctuations in complexes 1KZN-Pyr, 3HUN-Pyr, and 7KCY-Pyr. Eigenvalues and variance are inversely related, with complex 5TZ1-Pyr having the lowest eigenvalue. The covariance matrix illustrated correla-tions between complex residues, with red indicating strong correlations, white indicating uncorrelated movement, and blue indicating anti-correlations. Elastic network protein maps highlight associations between atoms, with darker areas representing more rigid parts of the molecule.

# Discussion

The synthesis of 5-(4-(dimethylamino)phenyl)-3-phenyl-4,5-dihydro-1H-pyrazole-1-carboxamide closely resem-bles the procedure reported in the previous study by (Sehmi et al., 2020) for the formation of the chalcone derivative, with both studies employing similar reac-tants and basic conditions. However, this study notably achieves a respectable 77% yield for the final com-pound, whereas the yield in the previous work remains unspecified.

Results indicated varying degrees of inhibition by pyrazoline carboxamide at different concentrations. *L. monocytogenes* and *C. albicans* were more sensitive to pyrazoline carboxamide compared to *E. coli*, *S. aureu*, and *P. aeruginosa*. Gentamicin exhibited significant inhibition against *E. coli* and *S. aureu*, while other anti-biotics displayed moderate to limited efficacy. These findings suggest that pyrazoline carboxamide holds promise as an antimicrobial agent, especially against *L. monocytogenes* and *C. albicans*. These results align with previous research reported that several drug-like compounds including indazoles, pyrazoles, and pyra-zolines as key heterocyclic units, synthesized in a flow-through mode, were found to possess significant

antibacterial potency against clinical and multi-drug resistant bacterial strains of the genera Staphylococcus and Enterococcus (Burke et al., 2023). Additionally, investigated the antibacterial activity against Gram-positive and Gram-negative bacteria of new series of Schiff-based thiazole-pyrazoline hybrids using ZnO nanoparticles with a more environmentally friendly and effective approach, showing better activity against *P. aeruginosa* and *E. coli* compared to amoxicillin (14.3 ± 2.5 and 14.7 ± 0.6 mm respectively; Zelelew et al., 2022). A study on the *in vitro* antibacterial activity of the synthesized [5-(furan-2-yl)-phenyl]-4,5-carbothioamide-pyrazolines was evaluated by the disk diffusion test, and then by the minimum inhibitory concentration of two Gram-positive and two Gram-negative bacteria such as *Aeromonas hydrophila*, *Yersinia enterocolitica*, *L. monocytogenes* and *S. aureus*, revealed a promising anti-bacterial activity compared to gentamicin and tetra-cycline (Rani et al., 2012).

Moreover, the synthesized pyrazoline carboxamide compound, holds promise for drug development due to its favorable physicochemical attributes, including molecular weight, composition, and aromaticity, posi-tioning it within a suitable molecular framework (Ahmad et al., 2023). Its moderate lipophilicity sugg-ests an ability to traverse both aqueous and lipid environments, vital for effective distribution and mem-brane permeation (Lipinski, 2001). Additionally, the compound demonstrates high gastrointestinal absorp-tion potential and blood-brain barrier permeability, signifying its capacity to enter the systemic circulation and potentially target the central nervous system (Pardridge, 2012). While its adherence to drug-likeness criteria is encouraging (Lipinski, 2001), the presence of potentially toxic substructures necessitates thorough safety evaluation before considering it for clinical use (Baell and Holloway, 2010). These findings underscore the compound's potential as a therapeutic candidate, but further scrutiny and toxicity assessments, as perfor-med using the eMOLTOX web tool, are imperative to ensure both its efficacy and safety in drug development (Ji et al., 2018). Furthermore, a comprehensive analysis of the binding interactions between the new pyrazoline compound and various antimicrobial target proteins has been investigated. The study assesses the strength of these interactions through estimated binding free energy, highlighting the binding affinities of Pyr com-pared to established standard inhibitors. The results reveal that Pyr exhibits variable binding affinities for different proteins, with specific amino acid residues involved in these interactions. Notably, Pyr exhibits high binding affinity to certain proteins, such as -8.4 kcal/mol for PDB ID 5TZ1. These results highlight the complex and contextual nature of Pyr's interactions with antimicrobial target proteins, providing valuable insights for drug design and optimization in the search for improved antimicrobial effects (Rossiter et al., 2017, Kleandrova and Speck-Planche, 2020). Finally, The

results of the IMODS analysis encompassing deformability, factor B, eigenvalues, variance map, correlation matrix, and elastic network model collectively provide a nuanced view of the structural dynamics of a biological macromolecule (López-Blanco et al., 2014). Deformability values indicate regions prone to flexibility, often associated with vital functional sites. B-factors reveal the extent of atomic thermal vibrations, highlighting regions where mobility is pronounced (Sun et al., 2019). Eigenvalues give insight into vibrational modes, emphasizing the rigidity or flexibility of the molecule. Variance maps graphically describe regions with high or low atomic fluctuations, providing clues about crucial dynamic areas (Mishra and Jernigan, 2018). The correlation matrix reveals functional interactions and structural connections, while the elastic network model simplifies interactions to predict collective movements (Liu, 2022). Interpreting these results not only helps understand the intrinsic behavior of the molecule but also highlights its functional relevance within biological systems, making this information invaluable for structural biology and drug discovery. NMA analysis of docked complexes was presented in Supplementary Figure 1. Affine arrows of two colors indicate mobility or movement direction, with longer arrows indicating greater movement. Deformability and factor B provide mobility profiles of anchored proteins. The deformability and B-factors of the complexes illustrate peaks corresponding to protein deformability regions, with higher peaks representing regions of high deformability (Sumera et al., 2022). The highest peaks are recorded for complex 1KZN-pyrazoline carboxamide, followed by 3HUN-pyrazoline carboxamide and 7KCY-pyrazoline carboxamide, which exhibit high deformability, while complex 5TZ1-pyrazoline carboxamide shows lesser deformability. B-factor diagrams provide a comparison between the NMA and PDB fields of the complexes. Complex 5TZ1-Pyr had a consistent B-factor score, but 1KZN-pyrazoline carboxamide, 3HUN-pyrazoline carboxamide, and 7KCY-pyrazoline carboxamide fluctuated more, each having significant peaks. Eigenvalues and variance are inversely related to each normal mode (López-Blanco et al., 2014). The target protein's variance graph displays individual variance with purple bars, while green bars represent cumulative variance. Eigenvalues describe the rigidity of movement, directly related to the energy needed to flex the protein (Quezada et al., 2017). The protein structure deforms most efficiently at a shorter energy range (May and Zacharias, 2008). Eigenvalue and variance map are inversely related (Szczepankiewicz et al., 2016). Complex 5TZ1-Pyr had the lowest eigenvalue of 1.973543e-05, followed in ascending order by values of 2.185665e-05, 8.826441e-05, and 5.30424e-04 for 1KZN-pyrazoline carboxamide, 3HUN-pyrazoline carboxamide, and 7KCY-pyrazoline carboxamide respectively. The covariance matrix of the complex shows correlations between complex residues. The red color of the matrix

illustrates the good correlation between residues, while white indicates uncorrelated movement. Additionally, the blue color indicates anti-correlations. Greater correlation signifies higher complexity (Kumar et al., 2014). Elastic network protein maps show associations between atoms, with darker gray areas indicating more rigid parts (Abdelli et al., 2021).

## Conclusion

The synthesized pyrazoline carboxamide compound showed potent antimicrobial activity, notably against *L. monocytogenes* and *C. albicans*. Its confirmed structural integrity, favorable drug characteristics, and promising molecular interactions indicate that it could be a compelling candidate for drug development.

## Financial Support

## Ethical Issue

The study protocol was approved the Institutional Ethical Committee

## Conflict of Interest

Authors declare no conflict of interest

## References

Abdelli I, Hassani F, Bekkel Brikci S, Ghalem S. *In silico* study the inhibition of angiotensin converting enzyme 2 receptor of COVID-19 by *Ammoides verticillata* components harvested from Western Algeria. J Biomol Struct Dyn. 2021; 39: 3263-76.

Ahmad I, Khan H, Serdaroğlu G. Physicochemical properties, drug likeness, ADMET, DFT studies, and *in vitro* antioxidant activity of oxindole derivatives. Comput Biol Chem. 2023; 104: 107861-80.

Aslam B, Wang W, Arshad MI, Khurshid M, Muzammil S, Rasool MH, Nisar MA, Alvi RF, Aslam MA, Qamar MU. Antibiotic resistance: A rundown of a global crisis. Infect Drug Resist. 2018; 11: 1645-58.

Baell JB, Holloway GA. New substructure filters for removal of pan assay interference compounds (PAINS) from screening libraries and for their exclusion in bioassays. J Med Chem. 2010; 53: 2719-40.

Burke A, Di Filippo M, Spiccio S, Schito AM, Caviglia D, Brullo C, Baumann M. Antimicrobial evaluation of new pyrazoles, indazoles and pyrazolines prepared in continuous flow mode. Int J Mol Sci. 2023; 24: 5319-31.

Chen H, Bajorath J. Designing highly potent compounds using a chemical language model. Sci Rep. 2023; 13: 7412-23.

Daina A, Michielin O, Zoete V. SwissADME: A free web tool to evaluate pharmacokinetics, drug-likeness and medicinal

chemistry friendliness of small molecules. Sci Rep. 2017; 7: 42717.

Daisley B, Koenig AD, Engelbrecht K, Doney L, Hards K, Al KF, Reid G, Burton JP. Emerging connections between gut microbiome bioenergetics and chronic metabolic diseases. Cell Rep. 2021; 37: 110087-106.

Ebenezer O, Shapi M, Tuszynski JA. A review of the recent development in the synthesis and biological evaluations of pyrazole derivatives. Biomedicines 2022; 10: 1124-81.

Ignatov I. Antimicrobial activity of colloidal nanosilver 24 ppm *in vitro*. Bulg Chem Commun. 2021; 53: 365-70.

Ji C, Svensson F, Zoufir A, Bender A. eMolTox: Prediction of molecular toxicity with confidence. Bioinformatics 2018; 34: 2508-09.

Kleandrova VV, Speck-Planche A. The QSAR paradigm in fragment-based drug discovery: From the virtual generation of target inhibitors to multi-scale modeling. Mini Rev Med Chem. 2020; 20: 1357-74.

Kumar K, Anbarasu A, Ramaiah S. Molecular docking and molecular dynamics studies on β-lactamases and penicillin binding proteins. Mol Biosyst. 2014; 10: 891-900.

Lake KM, Rankin SC, Rosenkrantz WS, Sastry L, Jacob M, Campos DD, Maddock K, Cole SD. *In vitro* efficacy of 0.2% and 0.4% sodium oxychlorosene against meticillin-resistant *Staphylococcus pseudintermedius*. Vet Dermatol. 2023; 34: 33-39.

Li B, Webster TJ. Bacteria antibiotic resistance: New challenges and opportunities for implant-associated orthopedic infections. J Orthop Res. 2018; 36: 22-32.

Lipinski B. Pathophysiology of oxidative stress in diabetes mellitus. J Diabetes Complicat. 2021; 15: 203-10.

Liu Z. Principal component analysis and normal mode analysis of elastic network models and their applications to myosin motor proteins. Doctoral dissertation. Wayne State University. 2022, pp 2023.

López-Blanco JR, Aliaga JI, Quintana-Ortí ES. Chacón P. iMODS: Internal coordinates normal mode analysis server. Nucleic Acids Res. 2014; 42(W1): W271-76.

May A, Zacharias M. Energy minimization in low-frequency normal modes to efficiently allow for global flexibility during systematic protein–protein docking. Proteins: Struct Funct Bioinf. 2008; 70: 794-809.

Mishra SK, Jernigan RL. Protein dynamic communities from elastic network models align closely to the communities defined by molecular dynamics. PLoS One. 2018; 13: e0199225.

Pardridge WM. Drug transport across the blood–brain barrier. J Cereb blood flow Metab. 2012; 32: 1959-72.

Quezada AG, Díaz-Salazar AJ, Cabrera N, Perez-Montfort R, Pineiro A, Costas M. Interplay between protein thermal flexibility and kinetic stability. Structure 2017; 25: 167-79.

Rani M, Yusuf M, Khan SA. Synthesis and *in-vitro*-antibacterial activity of [5-(furan-2-yl)-phenyl]-4,5-carbothioamide-pyrazolines. J Saudi Chem Soc. 2012; 16: 431-36.

Rattanasuk S, Boongapim R, Phiwthong T. Antibacterial activity of *Cathormion umbellatum*. Bangladesh J Pharmacol. 2021; 16: 91-95.

Rossiter SE, Fletcher MH, Wuest WM. Natural products as platforms to overcome antibiotic resistance. Chem Rev. 2017; 117: 12415-74.

Sehmi A, Ouici H, Guendouzi A, Ferhat M, Benali O, Boudjellal FJJS. Corrosion inhibition of mild steel by newly synthesized pyrazole carboxamide derivatives in HCl acid medium: Experimental and theoretical studies. J Electrochem Soc. 2020; 167: 155508-27.

Sumera F, Anwer M, Waseem A, Fatima N, Malik A, Ali, Zahid A. Molecular docking and molecular dynamics studies reveal secretory proteins as novel targets of temozolomide in glioblastoma multiforme. Molecules 2022; 27: 7198-214.

Sun Z, Liu Q, Qu G, Feng Y, Reetz MT. Utility of B-factors in protein science: Interpreting rigidity, flexibility, and internal motion and engineering thermostability. Chem. Rev. 2019; 119: 1626-65.

Sundar RDV, Arunachalam S. Effect of endophytic fungi Daldinia eschscholtzii against multidrug resistant pathogens. Bangladesh J Pharmacol. 2023; 18: 17-23.

Szczepankiewicz F, van Westen D, Englund E, Westin CF, Ståhlberg J, Lätt PC. Sundgren and M. Nilsson. The link between diffusion MRI and tumor heterogeneity: Mapping cell eccentricity and density by diffusional variance decomposition (DIVIDE). Neuroimage 2016; 142: 522-32.

Trott O, Olson AJ. AutoDock vina: Improving the speed and accuracy of docking with a new scoring function, efficient optimization, and multithreading. J Comput Chem. 2010; 31: 455-61.

Venkataraman S, Jain S, Shah K, Upmanyu N. Synthesis and biological activity of some novel pyrazolines. Acta Pol Pharm. 2010; 67: 361-66.

Vică ML, Glevitzky M, Tit DM, Behl T, Heghedűş-Mîndru RC, Zaha DC, Ursu F, Popa M, Glevitzky I, Bungău S. The antimicrobial activity of honey and propolis extracts from the central region of Romania. 2021; Food Biosci. 41: 101-14.

Wan-Mohtar WAAQI, Ibrahim MF, Rasdi NW, Zainorahim N,Taufek NM. Microorganisms as a sustainable aquafeed ingredient: A review. Aquac. Res. 2022; 53: 746-66.

Zelelew D, Endale M, Melaku Y, Kedir F, Demissie TB, Ombito JO, Eswaramoorthy R. Synthesis, antibacterial, and antioxidant activities of thiazolyl-pyrazoline schiff base hybrids: A combined experimental and computational study. J Chem. 2022; 2022.

**Author Info**
Farouk Boudou (Principal contact)
e-mail: drfarouk.boudou@gmail.com